Int J Adv Manuf Technol (2008) 39:239–250
DOI 10.1007/s00170-007-1223-5

ORIGINAL ARTICLE

Ultrafast laser micromachining of 3C-SiC thin films for MEMS device fabrication

Ben Pecholt · Monica Vendan · Yuanyuan Dong · Pal Molian

Received: 5 May 2007 / Accepted: 28 August 2007 / Published online: 15 September 2007

Abstract Femtosecond pulsed laser (800 nm, 120 fs) micromachining of thin films of 3C-SiC (β-SiC) semiconductor deposited on silicon substrate was investigated as a function of pulse energy (0.5 μJ to 750 μJ). The purpose is to establish suitable laser parametric regime for the fabrication of high accuracy, high spatial resolution and thin diaphragms for high-temperature MEMS pressure sensor applications. Etch rate, ablation threshold and quality of micromachined features were evaluated. The governing ablation mechanisms, such as thermal vaporization, phase explosion, Coulomb explosion and photomechanical fragmentation, were correlated with the effects of pulse energy. The results show that the etch rate is higher and the ablation threshold is lower than those obtained with nanosecond pulsed excimer laser ablation, suggesting femtosecond laser's potential for rapid manufacturing. In addition, the etch rates were substantially higher than those achievable in various reactive ion and electrochemical etching methods. Excellent quality of machined features with little collateral thermal damage was obtained in the pulse energy range (1–10 μJ). The leading material removal mechanisms under these conditions were photomechanical fragmentation, ultrafast melting and vaporization. At very low pulse energies (<1 μJ), nanoscale material removal has occurred with the formation of nanoparticles that is attributed to Coulomb explosion mechanism. The effect of assist gas on the process performance at low and high energy fluences is also presented.

B. Pecholt · M. Vendan · Y. Dong · P. Molian (✉)
Department of Mechanical Engineering, Laboratory for Lasers, MEMS and Nanotechnology, Iowa State University, Ames, IA 50011-2161, USA
e-mail: molian@iastate.edu

Keywords Femtosecond laser · Micromachining · Hard material · Material removal mechanisms · Semiconductor

1 Introduction

Silicon is the current material dominating the microelectronics and MEMS industries today. Silicon carbide (SiC), however, has superior properties compared to silicon in terms of bandgap, high-temperature resistance, thermal conductivity, mechanical strength and stiffness, all of which strongly favor it for its utility as sensors, actuators and power devices. SiC exists in over 170 different polytypes and each type has its own distinct set of electronic properties. However, only three polytypes, namely 3C, 4H and 6H, are acceptable for use as semiconductors because they can be grown as single crystal wafers. 3C-SiC is preferred for its ability to provide the highest speed of electron and hole transport in the crystal while 6H-SiC and 4H-SiC are desired for their wide bandgaps. All polytypes are extremely hard, chemically inert and have high thermal conductivity. For MEMS devices, 3C-SiC serves as the best mechanical substrate due to its extreme hardness and stiffness. However, there are formidable challenges in the crystal growth of high quality, bulk wafers of 3C-SiC that prevents its commercial production. Hence thin films of 3C-SiC are widely used for fabricating MEMS devices. The 3C polytype, also known as β-SiC, exhibits cubic structure, crystallizes in ZnS-type structure and epitaxially grows as thin film on silicon substrate. It also requires much lower substrate temperature (1,500°C or less) than other polytypes in chemical vapor deposition (CVD). In contrast, the 6H-SiC (hexagonal) and 4H-SiC (tetragonal) would not

grow as thin film on any substrate except on its own and also requires very high temperature (2,000°C) for growth.

CVD, sputtering, metal-organic CVD, atomic layer epitaxy, molecular beam epitaxy, and pulsed laser deposition are the current techniques used to grow amorphous, single and polycrystalline forms of 3C-SiC thin films [1, 2]. MEMS devices, such as pressure sensors, accelerometers, lateral resonators, gas sensors and micromotors for use in harsh environments, are fabricated by surface micromachining of 3C-SiC thin films [3–5]. Conventional surface micromachining of single crystalline SiC film on silicon is difficult to accomplish in contrast to polycrystalline and amorphous SiC layers. Poly-SiC is generally grown on poly-Si layer or deposited on SiO_2 layer. The SiC is the structural layer while the poly-Si or SiO_2 is the sacrificial layer. KOH and HF are used to release the SiC microstructures from poly-Si and oxide layers, respectively. One critical microfabrication issue is that the traditional wet etching does not work well for SiC. Patterning techniques based on photolithography and reactive-ion-etching (RIE) with SF_6/O_2 plasma, SF_6/O_2 inductively coupled plasma (ICP) and deep reactive ion etching (DRIE) processes were customarily used to etch SiC thin films, however, at the expense of very slow etch rates (few nm per second). Photo- and electro-chemical etching processes can also be used where SiC is first anodized to form a deep porous layer and subsequently removed through thermal oxidation followed by a dip in HF; however, these processes suffer from poor etch selectivity, low etch rates and cumbersome process steps [4].

In the micro-manufacturing industry, the laser is being established as an indispensable tool because of the benefits such as higher etch rates, easier automation and better quality features. Excimer lasers are extensively used for micromachining polymers and ceramics while Nd:YAG lasers are used for microdrilling and marking of semiconductors and metals. However, these lasers (nanosecond to millisecond pulses) are not well suited for precise microstructuring due to thermal or mechanical damages (recast layers, burrs and cracks, etc.), limiting the achievable precision and quality. These shortcomings have spurred the development of ultrafast (pico- and femtosecond) lasers, which deliver enhanced precision and cleanliness of machined features by minimizing collateral damage, plasma effects and thermal diffusion [6–9].

Femtosecond (fs) pulsed lasers are emerging as tools for microfabrication of all types of materials that are used in biomedical, micoelectronics, photonics and MEMS industries. The unique characteristics of ultrafast lasers over longer-pulsed lasers are multiphoton ionization and absence of energy transfer from electrons to the lattice, leading to deterministic and reproducible ablation; negligible thermal damage; and high etch rates (0.01 to 1 μm/pulse). These unique advantages make femtosecond lasers promising for the fabrication of a variety of materials, such as low melting point polymers, high thermal conductivity metals, wide bandgap dielectrics, and semiconductors that are otherwise difficult to perform by conventional tools.

Applications of femtosecond laser micro-structuring of channels and trenches have been demonstrated in materials such as fused silica, silicon, and pyrex [10]. Microfluidic channels as deep as 50 microns were successfully machined in Si(100) at 395 nm with a fluence of 0.6 J/cm^2 [10]. Micro-structures on alumina ceramic, which is typically affected by tool wear, were machined up to 150 μm deep using a scanned intensity in the range of 7–50 W/cm^2 and only a 2 μm thick recast layer was observed at the bottom of the structure [11]. Femtosecond lasers with their minimal thermal effects have been successfully used to create microstructures in aluminum with quality side walls despite its high thermal conductivity and low melting point [12, 13]. Damaging fs-laser effects on metals were also shown to be mitigated with the use of helium as an assist gas [12–14] The fs-laser has already been demonstrated to have a "non-thermal" ablation mechanism for micro-structuring of 3C-SiC thin film [5]. Reported use of femtosecond pulses to successfully drill holes in 3C-SiC bulk wafers [15] and trenches up to 60 μm deep in 6H-SiC [16] suggests that ultra-short pulses are well suited for machining bulk silicon carbide as well as 3C-SiC thin film [5]. In this paper, we present the results of a systematic study of the effects of pulse energy on etch depth, quality of machined features and material removal mechanisms in 3C-SiC thin films on Si(100) substrate using a Ti:sapphire femtosecond pulsed laser.

2 Experimental details

Atmospheric pressure chemical vapor deposition (AP-CVD) system was employed to grow 1-μm thin films of 3C-SiC on 100-mm diameter, 500-μm thick (100) silicon substrates in a cold-wall, vertical-geometry, RF induction-heated, atmospheric pressure CVD reactor. Prior to deposition, the reaction chamber was pumped down to a pressure of 200 mtorr and then backfilled with ultra-high purity argon to 760 torr to remove the oxide impurities. Ultra-high purity hydrogen (carrier gas), propane (15% hydrogen) and silane (5% hydrogen) were then introduced into the chamber. The chemical reaction took place at 1,360°C. A three-step deposition process was used, beginning with an in situ hydrogen etch of oxides and contaminants, followed by the formation of a carbonized layer on the substrate surface, and ending with the film growth. The film growth rate was about one μm per hour. Details of this technique are described elsewhere [17].

A Ti:sapphire laser (Spectra Physics, Hurricane X), based on the chirped pulse amplification (CPA) technique, was used to create microholes and microchannels in 3C-SiC thin films. The output beam has the specifications of wavelength of 800-nm, repetition rate of 1-kHz, and pulse width of 120-fs. The 6-mm diameter laser beam with a Gaussian energy distribution was circularly polarized, expanded to twice the size using an up collimator, and steered by a 45° mirror. The beam was then transmitted through neutral density filter to reduce the pulse energy and then focused by a reflective objective lens to a spot size of 4±1 μm. In experiments with higher pulse energies (>100 μJ), a plano-convex lens (50 mm focal length) was us,ed giving rise to a spot size of 40±5 μm. The pulse energy was varied from 1 μJ to 750 μJ. For ablation rate studies, single-shot mode was used with energy fluence in the range 0.1 to 20 J/cm^2.

3C-SiC thin film deposited samples were cleaned with tricholorethylene, acetone and deionized water consecutively and then mounted on a computer controlled x-y stage (Coherent Lab Motion Series), which has a resolution of 1 μm. The movement of the stage was programmed in the lab motion software to produce the desired laser path. The beam was used in the direct-writing mode to follow the program. Helium was used as a shield/assist gas to eject vaporized material, produce clean cuts and protect the lens. In some experiments, air was also used as the assist gas to identify the effects of self-focusing. After laser micromachining, a few samples were etched in KOH solution for about 5–10 minutes to remove the recast layers. Scanning electron microscope, atomic force microscope and surface profilometer were then used to examine the ablated regions and measure the etch depths.

3 Results and discussion

Etch rate and ablation threshold Etch rate is an overriding consideration in SiC micromachining because of its chemical inertness and extreme hardness. Figure 1 shows the etch depth per pulse as a function of energy fluence based on experiments using 50 mm focal length lens (40 μm spot size). The non-linear dependence of ablation rate with fluence is attributed to multiphoton ionization. These etch rates are much higher than those obtained with nanosecond-pulsed excimer (193 nm, 248 nm) lasers and comparable to 400-fs (1026 nm) laser in the ablation of 3C-SiC bulk wafers [15]. Similarly, the etch rates are greater than maximum achievable (7 nm/s) in RIE, electron cyclotron resonance and magnetron-enhanced RIE [18, 19]. Higher etch rates observed in ultrafast laser ablation are attributed to multiphoton absorption and reduced thermal diffusion. In the ns-laser pulse regime, photon energy must exceed the summation of band gap (3 eV for SiC) and electron affinity (4.5 eV for SiC) to excite the electrons and cause bond scission. Although 800-nm photons cannot meet such energy requirements, the multi-photon absorption associated with extreme intensity of femtosecond pulse and the presence of lattice defects in 3C-SiC thin films are responsible for bond breaking and subsequent emission of electrons and ions.

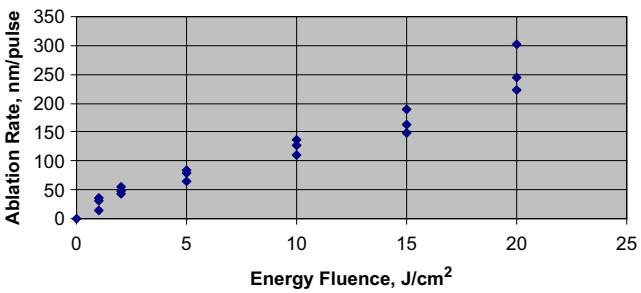

Fig. 1 Single-shot ablation rates of 3C-SiC thin films

Threshold ablation is a characteristic dependent on the wavelength, pulse width and type of material. It is ideally defined as the energy fluence at which irreversible damage occurs in the material by removing a monolayer of material. It is actually determined by visual examination, ablation depth measurement, plasma radiation monitoring etc. However in this study the ablation threshold was estimated by recording the diameter (D) and the depth of single-shot ablated craters using atomic force microscope and then using the following linear relationship between the square of the crater diameter and the logarithm of the laser fluence [20]:

$$D^2 = 2w_0^2 1n(F_o/F_{th}) \quad (1)$$

where F_{th} = ablation threshold and $2w_o$ = spot size. A plot of the square of damage diameter, D^2, against the logarithm of energy fluence was made to obtain both the spot size (slope of line) and ablation threshold (the extrapolation of D^2 to zero value). The spot size, $2w_o$, was 40 μm and ablation threshold was 0.7 J/cm^2. For comparison, the ablation threshold of bulk 3C-SiC by 400-fs (1026 nm) and 34 ns (248 nm) lasers were 0.55 J/cm^2 and 1.5 J/cm^2 respectively. The lower threshold in ultrafast laser compared to 248 nm excimer laser is a consequence of multiphoton absorption effect.

Effect of pulse width Figure 2 shows the scanning electron microscope (SEM) images of microchannels produced in 3C-SiC thin films using the 120-fs pulsed Ti:sapphire (800 nm) and 90-ns pulsed Nd:YAG (1064 nm) lasers. There were large amounts of debris and recast layer in the ns-pulsed laser micromachined region. The coating seems to have discolored and also delaminated away from the kerf. The laser beam has cut through the silicon substrate

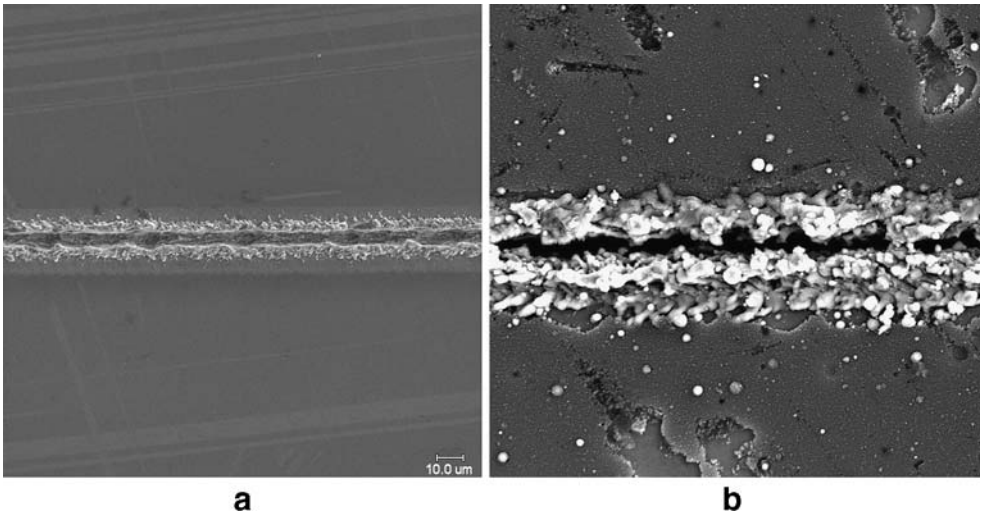

Fig. 2 Microchannels generated by (**a**) 120-fs laser (**b**) 90-ns laser under identical conditions: pulse energy 60 μJ, spot size 4 μm, speed 1000 μm/s

and made significant collateral thermal damages. In addition, a rough surface morphology, characterized by jagged protrusions, can be seen. In contrast, the fs-laser machined region exhibits narrow kerf, relatively small amount of recast layer and almost no spatter. Thus, rapid energy deposition and its localization lead to fabrication of microstructures with high quality and reproducibility.

Laser-material interactions The physical mechanisms of femtosecond laser ablation of wide bandgap semiconductors such as SiC remains poorly understood. For example, the roles played by defects and impurities on the energy absorption and dissipation are not yet made clear. In general, at high intensities ($>10^{13}$ W/cm^2) of femtosecond lasers, multiphoton absorption becomes considerably strong and seed electrons are not required to begin ionization. Multiphoton ionization and free electron heating occur in SiC during the femtosecond pulse duration and hence the lattice temperature remains unchanged. Laser energy is deposited much faster than the ability of the material to dissipate energy, thus a state of extreme non-equilibrium is reached and free electrons are generated ionizing the material into dense plasma. These plasmas have been shown to have highly reflective, metal-like properties [21]. Even plasmas formed on optically transparent materials have been shown to exhibit reflective properties [22]. Subsequent laser-plasma interaction causes phase change and material ejection (ablation). Additionally the free electrons associated with the ionization of the material are responsible for absorption of photons and defocusing of the beam [23]. Ionization of the gases used as a propagation medium in laser processing also result in a number of unfavorable consequences due competing phenomena, such as self-focusing and de-focusing [23]. Ionization-induced defocusing occurs when the gas medium results in plasma at the leading edge of the beam [24, 25]. A higher degree of ionization occurs at the center of the beam due to Gaussian beam energy distribution resulting in a larger index of refraction on the axial center [24, 26]. This type of ionization takes place when the beam energy is at the ionization potential of the gas. When the laser intensity is increased to higher values than the plasma threshold, the plasma becomes more uniform and the non-linear index of refraction generates self-focusing [26]. Gases with a high ionization potential such as helium have been used at ambient pressures in beam propagation [12] to avoid self-focusing effects and as an assist gas to aid in plasma shielding resulting in a lower level of debris and diminished heat-affected-zone [12–14].

There are several mechanisms proposed for material removal in femtosecond laser ablation, which include normal melting [21], thermal vaporization [27], ultrafast laser melting [28–34], phase explosion [31–35], Coulomb explosion [36, 37] and photomechanical fragmentation [38–41] depending on laser intensity, pulse width, wavelength, number of pulses and material properties. Coulomb explosion, ultrafast melting and free electron heating arise in fast pace (femtosecond), while thermal vaporization and fragmentation occur at slow pace (nanoseconds) [21]. Phase explosion, normal melting and electron-lattice relaxation take place in the intermediate picosecond scale. In the case of wide bandgap semiconductors such as SiC, one or more of these mechanisms could be operative depending on energy fluence. In this work, the observations of machined features are grouped in three regimes on the basis of pulse energy and then used to identify the underpinning physical mechanisms of micromachining of 3C-SiC thin films.

High energy ablation Figures 3 and 4 show the microchannels and microholes produced by the femtosecond laser at much higher pulse energies (50 μJ to 750 μJ). The presence of large amounts of recast layer and spatter as well as sub-μm/pulse etch depth and rough surface suggests that thermal effects caused by phase explosion and vaporization

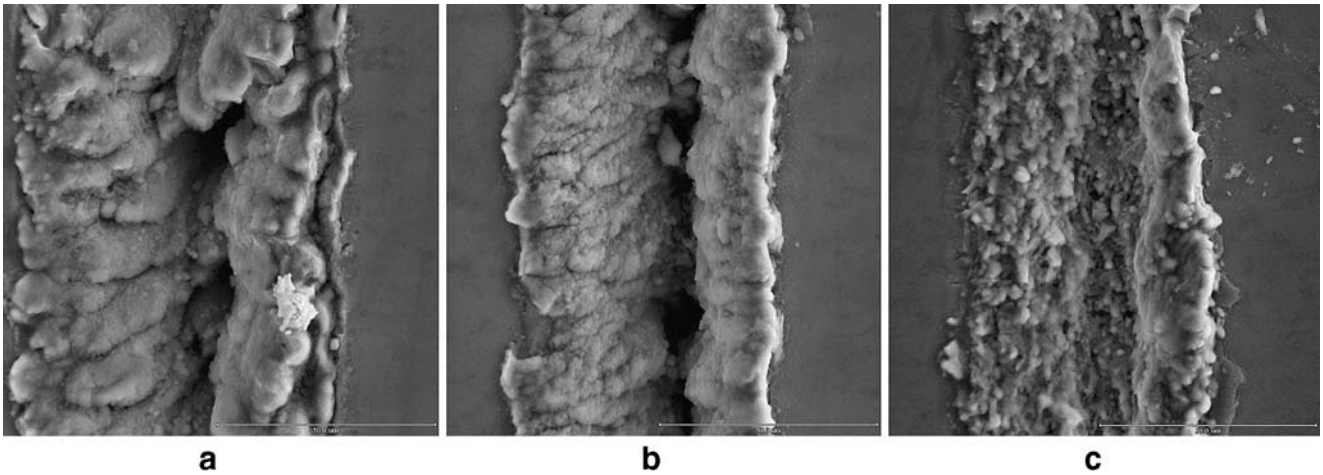

Fig. 3 Femtosecond laser micromachined channels in 3C-SiC thin films deposited on silicon at a speed of 1000 μm/s; (**a**) 750 μJ; (**b**) 500 μJ; (**c**) 250 μJ

mechanisms control the ablation. Phase explosion (PE), also known as explosive boiling or homogeneous nucleation of gas bubbles, precedes thermal vaporization. PE is a mechanism where the laser-irradiated matter enters the metastable region of the phase diagram (binodal or spinodal) by reaching the limit of thermodynamic stability and approaching the critical temperatures [42, 43]. When the temperature of the liquid approaches the critical point, the superheated liquid transforms into a mixture of liquid and vapor and undergoes evaporation at an excessive rate [44, 45]. Violent ejection of the mixture of vapor and liquid droplets occur from the sample surface due to the recoil force created by the momentum transfer. Evidence for the phase explosion mechanism in Fig. 4 is the presence of splashed material around the holes and high density of redeposited particulates. PE, accompanied by melt expulsion and collateral thermal damage, has been validated in femtosecond pulsed laser ablation of semiconductors [36]. PE generally removes small amount of material by vaporization. Thermal vaporization continues after phase explosion, causing large amount of material removal and forming the kerf. Although ultrafast lasers are expected to minimize such thermal effects, it appears that explosive vaporization accompanied by substantial melt formation does occur at high pulse energies, leading to poor quality cuts.

Low energy ablation Figure 5 a to c show the channels micromachined in 3C-SiC using low pulse energies (2–10 μJ). There are material fragments indicative of mechanical fracture and kerf pinpointing material loss through vaporization. In this regime, the mechanisms of material removal are believed to be a combination of ultrafast laser melting, vaporization, photomechanical fragmentation and Coulomb explosion (CE). Ultrafast melting of semiconductors at fluences above the damage threshold is theoretically proven as a non-thermal phase transition on a sub-ps time scale for semiconductors [21]. It begins with the develop-

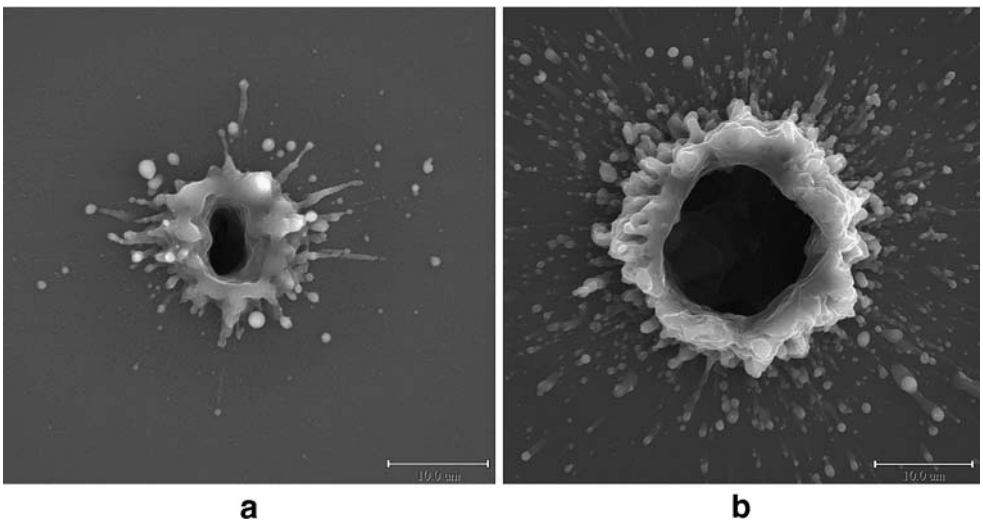

Fig. 4 Femtosecond laser micromachined holes in 3C-SiC thin films deposited on silicon with 30 pulses; (**a**) 50 μJ; (**b**) 200 μJ

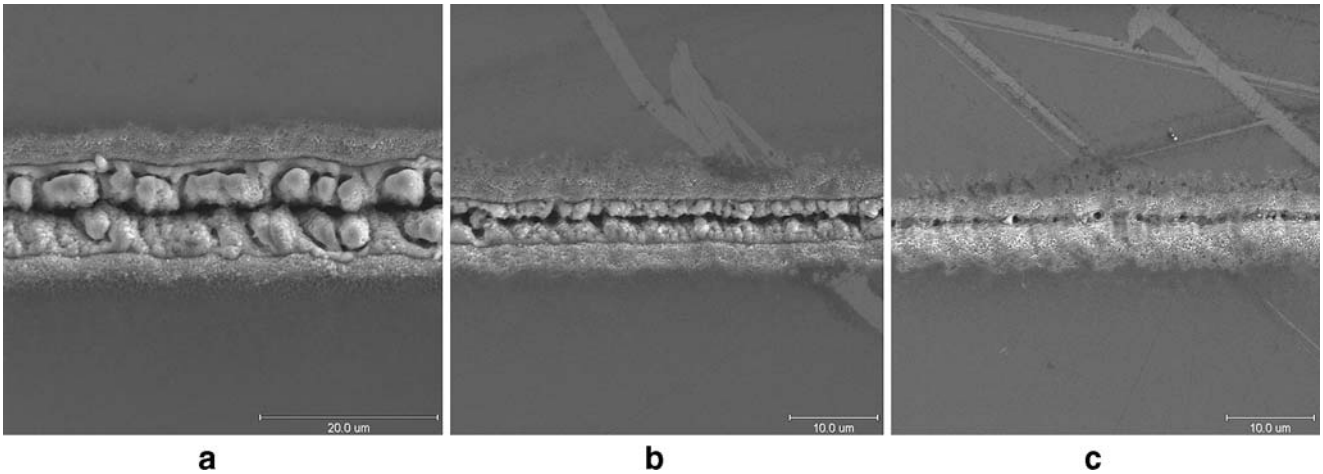

Fig. 5 Femtosecond laser micromachined channels in 3C-SiC thin films deposited on silicon at a speed of 20 μm/s; (**a**) 5 μJ; (**b**) 2.5 μJ; (**c**) 1.5 μJ

ment of metal-like phase due to the dense electron-hole plasma followed by bond softening and lattice destabilization due to a significant fraction of electrons jumping from valence band to conduction band. For example, steep gradients of the free electron density account for the depth of the non-thermally melted layer as 20–40 nm in Si [21]. Thermal melting, which takes place after ultrafast melting, produces much thicker melt layers. Thus ultrafast melting followed by normal melting and vaporization seems to be responsible for the formation of small kerf in Fig. 5. However the most dominant mechanism appears to be photomechanical fragmentation where the material disintegrates into large clusters as a result of mechanical stress imposed by the rapid thermal expansion of the surface. In this mechanism, thermoelastic stresses are developed by the rapid thermal expansion of the surface layers due to constant-volume heating; the relaxation of these stresses cause large values of non-uniform strain rates, leading to a strong increase in elastic energy that breaks the material into an ensemble of clusters [27]. This strain-induced fragmentation does neither require any phase change nor the crossing of metastability limits as in phase explosion. It differs from other photomechanical mechanisms, such as spallation and cavitation because it does not involve tensile stresses. Another intriguing feature in Fig. 5 is the presence of significant amounts of nanoscale/sub-μm particles near the lateral edges of the microchannels that are attributed to CE mechanism (see the next section for complete discussion).

Figure 6 shows the scanning electron microscope (SEM) images of 120 μm size micromotor-rotors processed at two pulse energies. The hole at the center is meant for assembling 25 μm diameter shafts. It may be noted that higher pulse energy ablation ruined the rotor structure by thermal damage, while the lower pulse energy ablation produced a reasonably well-defined profile with improved

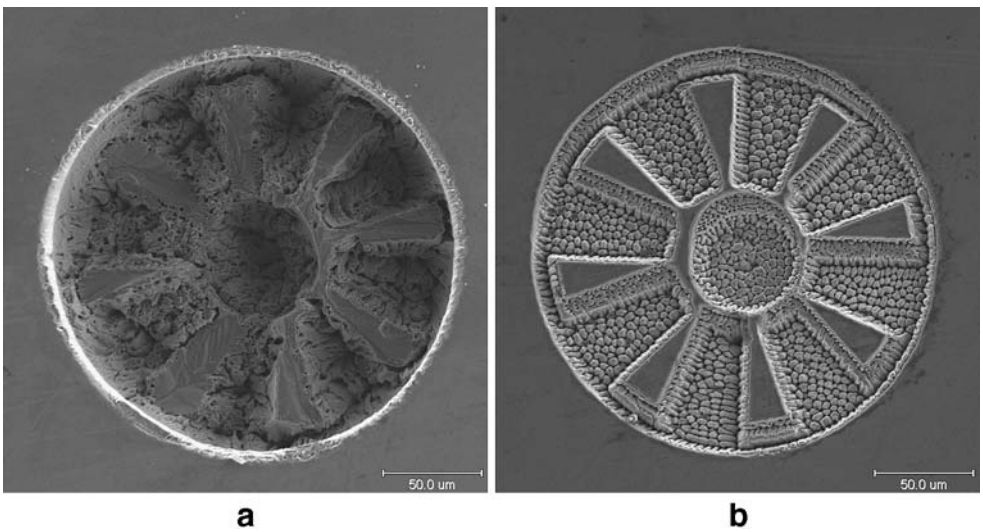

Fig. 6 Femtosecond laser micromachined rotor in 3C-SiC thin films deposited on silicon (**a**) 60 μJ; (**b**) 8 μJ

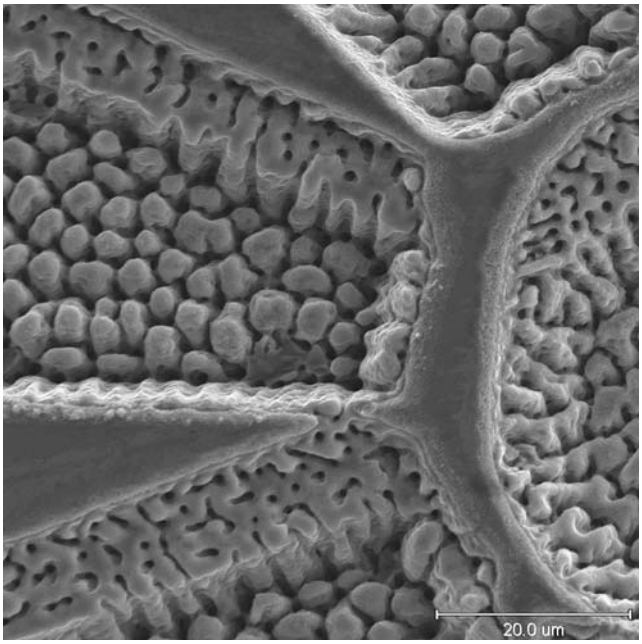

Fig. 7 High-magnification views of the center section of rotor displayed in Fig. 6 (**b**)

resolution, little contamination and minimal thermal damage. There is no evidence of typical thermal damages, such as recast layer, ripple, column and crack. Instead, a large number of loose fragments and tiny holes were noted in the center section of rotor (Fig. 7) probably caused by photomechanical fragmentation and vaporization respectively. Figure 8 shows an SEM micrograph of a salient-pole micromotor with stator and rotor having a gap of 2 μm between them. KOH etchant was used to remove the loose fragments and release the rotor part. Caution must be exercised during the etching process because the central portion (shaft) may also be etched out as it is much smaller in area than each arm of the rotor.

Very low energy ablation When the pulse energy was further reduced to less than 1.5 μJ, the ablation mechanisms appears to be exclusively of Coulomb explosion and photomechanical fragmentation. Figures 9 and 10 are the SEM images showing the effects of very low energy on the channel profiles. There is also evidence of the formation of nanoparticles on the sidewalls of etched profile. Figure 11 is a rotor fabricated using 1.2 μJ that shows much improved resolution and accuracy over the one fabricated at 8 μJ (Fig. 6 (b)). Actually the size of this rotor is even smaller than the one shown in Fig. 6 (b), inferring that low-energy processing is appropriate for fine structures with high resolution.

We contemplate Coulomb explosion (CE) as a possible mechanism for material removal in this regime because of the following characteristics: 1) time-of-flight analysis showed that the ions move at faster rate than in thermal vaporization; 2) etch rate is on the order of nanometer per pulse; 3) ablated surface contains a high density of nanoparticles. CE involves charge localization unlike phase explosion. Due to the capability of femtosecond laser in dumping large amounts of energy in short time, the laser pulse will excite the electrons through multiphoton and impact ionizations and emit the electrons from the surface and underlying regions, inducing strong ionization and leaving a high concentration of uncompensated ions. Essentially, the femtosecond laser creates a track of electron-hole pair excitations with a charge imbalance (because the mobility of holes is much smaller than that of the electrons). Hence the surface becomes electro statically unstable and electric field is generated. If the electric field strength exceeds that of the binding energy of atoms in the target, CE takes place. Intrinsically a non-thermal process, CE dominates at low pulse energy and usually removes a small fraction of the mass.

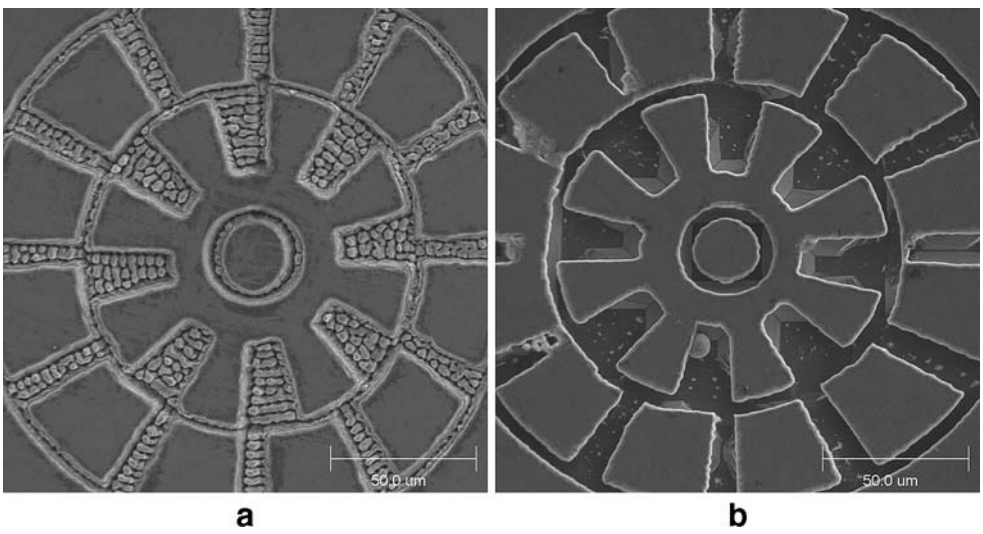

Fig. 8 Femtosecond laser micro-machined micromotor in 3C-SiC thin films deposited on silicon (**a**) After laser ablation; (**b**) Subsequent etching in KOH

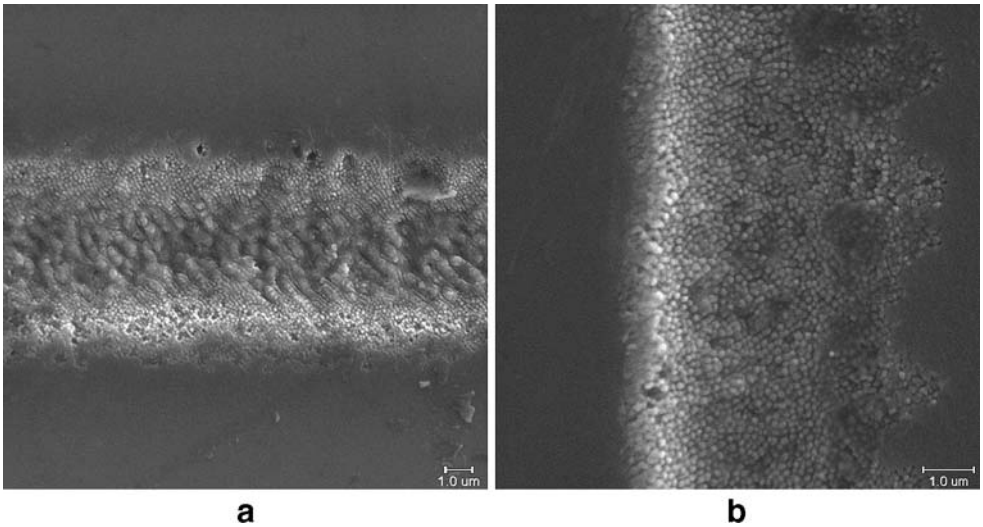

Fig. 9 Femtosecond laser micromachined channel at pulse energy of 1.2 μJ. Note the formation of 50–100 nm diameter nanoparticles at the edge. (**a**) Microchannel; (**b**) Edge of channel

CE has been experimentally proven to occur in aluminum oxide dielectrics under femtosecond laser irradiation with 800-nm laser wavelength at laser fluences only slightly above the ablation threshold [21, 46, 47]. However, the applicability of CE in ultrafast laser ablation of semiconductors remains controversial. For example, the electron dynamics calculations of surface charging profiles of dielectric Al_2O_3 (induced by 100-fs laser) provided a net surface charge (n_i-n_e) density of 7×10^{21} /cm^3 in contrast to silicon where the net accumulated positive charges during the 100-fs laser pulse is 200 times lower [48]. This difference was attributed to the higher electron mobility and higher density of available free electrons for semiconductors, causing effective screening. Stoian et al. [48] hypothesized that effective quenching of surface charging by bulk electrons do not permit CE to occur in semiconductors. However, recent experimental evidence suggests the occurrence of CE for Si (111) after 800-nm, fs-laser ablation at a higher energy fluence of 1.2 J/cm^2 because at lower fluences efficient electronic transport from the bulk counteracts the laser-induced charges [49].

Nanoparticle formation Figure 12 is a single-shot laser irradiated zone at very low pulse energy of 0.5 μJ showing the formation of nanoparticles. X-ray diffraction was used to characterize the crystalline structure and orientation while and Auger electron spectroscopy was used to identify the composition of nanoparticles. Figure 13 shows XRD patterns of both CVD and laser nanostructured 3C-SiC films exhibiting cubic (zinc-blende) structure. The (111), (200) and (400) reflection peaks are identified in the CVD deposited 3C-SiC thin films (Fig. 13 a). However after laser nanostructuring, the ratio of intensity of (111) to (200) peaks was sharply reduced while the FWHM of (200) became narrower. A strong preferred orientation along the <100> direction was observed, indicating the more stable

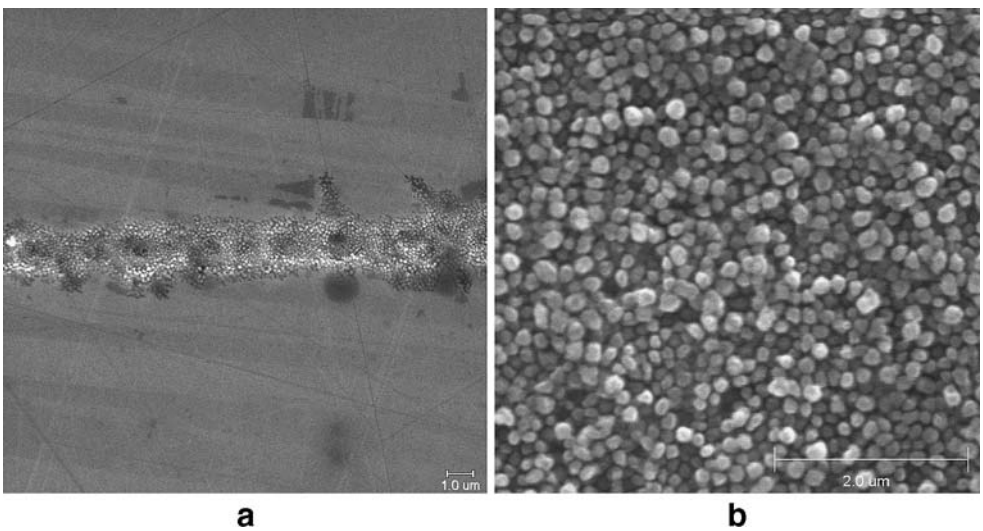

Fig. 10 Femtosecond laser micromachined channel at a pulse energy of 0.6 μJ. (**a**) Microchannel; (**b**) Structure within the channel

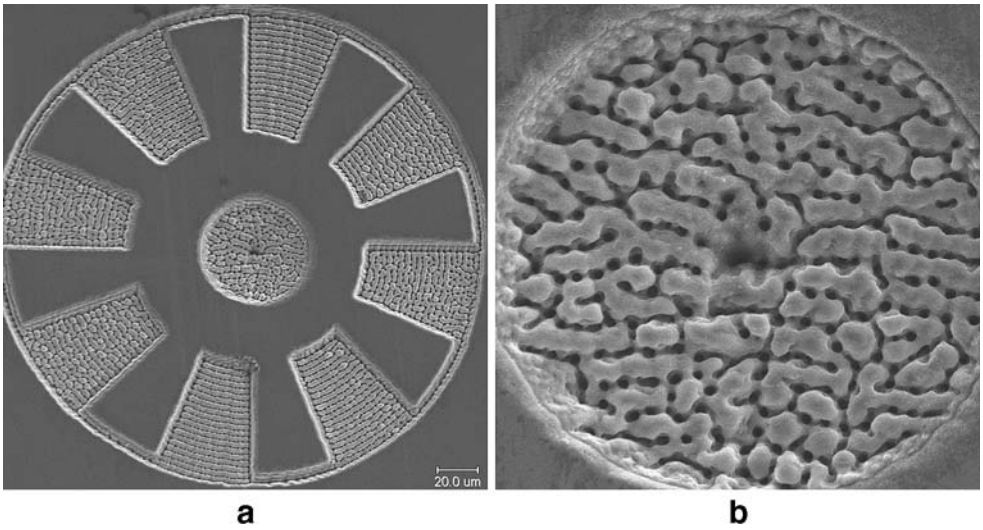

Fig. 11 Femtosecond laser micromachined rotor in 3C-SiC thin films deposited on silicon using a pulse energy of 1.2 μJ; (**a**) Rotor; (**b**) Magnified view of central portion

structure. The modification of crystalline orientation in nanoparticles is attributed to lattice arrangement resulted from increased lattice vibration due to lattice heating accompanying Coulomb explosion. Auger electron spectrometry (AES) was utilized to determine the CVD (un-irradiated) and nanoparticle (laser-irradiated) SiC films. Figure 14 shows the results. For the laser-irradiated film, an oxygen contamination was present, but it was rapidly reduced to trace amounts after 35 seconds of Ar ion etching. The CVD and post Ar-ion etched films were comparable in binding energy and intensity implying that the composition was unchanged.

Nanostructuring presented in this work has also been observed in ion sputtering of materials with highly charged ions at low impact energies [50, 51]. Molecular dynamics simulations of highly-charged-ion collisions on silicon surfaces have shown that CE accounts for the production of nanoscale structures and is in agreement with experimental findings [47]. Molecular simulations of ultrafast laser ablation of silicon at low fluences exhibit many similarities to the ion beam bombardment [52, 53]. The time scale for Coulomb explosion is found to be <1 ps. For laser pulse durations longer than 1 ps, ion emission can still occur but thermal excitation of the lattice will cause a phase explosion mechanism, leading to large amount of material removal and nanoscale structuring will be destroyed. In contrast to the nanosecond laser pulses, ultrafast pulses have an advantage of not interacting with the plume of ablated material since the pulse has ceased prior to the laser damage. Consequently, plume heating and shock-wave mechanisms do not account for nanoparticle formation.

Another possible mechanism of nanoparticle formation on the solid surfaces subjected to laser ablation is the

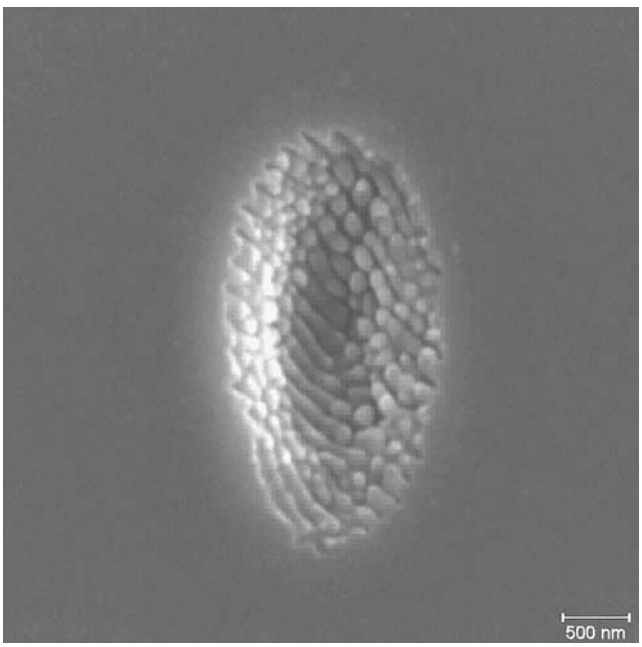

Fig. 12 Single-shot, femtosecond laser micromachined region in 3C-SiC thin films deposited on silicon (pulse energy=0.5 μJ)

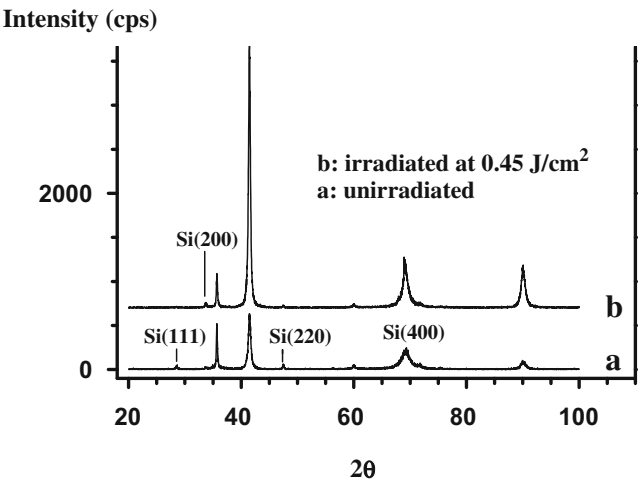

Fig. 13 X-ray diffraction spectra of 3C-SiC films of (a) CVD thin film and (b) Laser nanostructured thin film

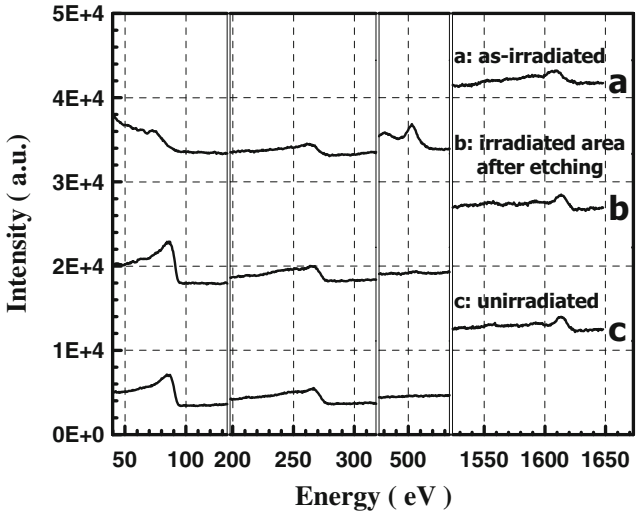

Fig. 14 Auger electron spectra of 3C-SiC films: a) Laser-irradiated at 0.45 J/cm^2; b) Laser irradiated and then Ar-ion etched; c) Un-irradiated

interference phenomenon leading to spatial periodic structures, known as ripples (also known as laser-induced periodic surface structure, LIPSS); this is believed to produce nanoparticles and nanopatterns on the surfaces [54–57]. Ripples emanate when incident or reflected or refracted laser light interferes with the scattered light from defects, roughness, or some sort of surface disturbance. Laser polarization plays a key role in the formation of ripple structure. Although the spacing between fringes is equal to the wavelength, recent experiments proved that the periods are substantially shorter than the wavelengths, leading to development of nanostructures in materials like TiN, InP, GaP and GaAs. The process begins with production of surface relief with shallow depressions and elevations and then continues with the formation of periodic nanochannels if linear polarization were used and the formation of self-organized array of nanoparticles if circular polarization were applied. Recent work showed the nanosecond pulsed 248-nm laser irradiation of Si at <1 J/cm^2 using a background of ultra-high pure helium generated the formation of nanoparticles in the form of linear arrays or strings depending on the type of polarization [57]. It is interesting to note the formation of such nanoparticles despite the use of high-energy fluence and long pulse, both of which tend to produce plasma and suppress the interference effects. Since these nanoparticles were created with a background of ultra-high pure helium, it could be an effect ascribed to gas phase condensation.

Effect of assist gases Experimental works that involve laser beam interaction with its propagation medium have shown the defocusing effects when the propagation medium (gas) is ionized by the leading edge of the beam [24, 25]. Researchers investigating femtosecond laser micromachining have emphasized the use of an inert gas to prevent the harmful effects of defocusing [12–14]. Micromachining of holes in copper showed that helium was a better gas medium for beam propagation than air, neon, and nitrogen. Use of helium as an assist gas resulted in improved sidewall quality, lower debris redeposition, and minimal thermal damage [14]. Similar studies on the effects of laser micro-structuring of trenches in aluminum revealed that helium markedly improved the quality as compared to ambient atmosphere [12], argon and nitrogen [13]. The exact mechanism by which helium prevents the redeposition of debris is not fully understood; however, it has been suggested that the recoil pressure caused by the hot plasma prevents debris from leaving the ablated area [14]. For near-infrared femtosecond pulses, use of helium as an assist gas for aluminum is more effective at lower fluences [12]. When the energy fluence was reduced to near threshold, nanometer-sized aluminum single crystal spheres were formed and carried away by the assist gas [12].

In the present work, ultrafast laser interactions with 3C-SiC were evaluated with the aid of helium as an assist gas and compared to those of ambient atmosphere. At low pulse energy of 0.2 μJ the formation of nanoparticles within the irradiated area has occurred; this was independent of the type of assist gas being ambient or helium assist gas. The implication is that the formation of nanoparticles at low fluence is not caused by oxidation. In low pulse energy regime that corresponds to a fluence much lower than the ionization fluence of air, the assist gases did not play a significant role. This was in agreement with the previous work [14]. However it was found at higher pulse energies, where thermal effects were significant, that the use of helium showed significant improvement in quality such as minimal recast layer over ambient atmospheric conditions.

4 Conclusion

Ultrafast laser micromachining of CVD-deposited single crystalline 3C-SiC thin film on silicon substrate was investigated as a function of pulse energy for the purpose of determining the optimum pulse energy for the fabrication of MEMS devices. The results were correlated with the underlying physical mechanisms. Higher pulse energies generated significant amount of recast layer and damaged fragments while lower pulse energies (<0.5 μJ) are not sufficient to ablate the material to the desired depth. High resolution, damage-free features were produced at low pulse energy (1–10 μJ). This study demonstrates that the femtosecond pulsed laser ablation has excellent potential for SiC micromachining and has a superior edge over

traditional reactive ion etching and electrochemical etching methods.

Acknowledgements The authors would like to acknowledge the National Science Foundation (NSF) for supporting this research work under the grant DMI-0619115. Thanks are also due to Dr. Chris Zorman of Case Western Reserve University for providing CVD-deposited thin film wafers.

References

1. MRS Bulletin (1997) Silicon carbide electronic materials and devices. Vol. 22(3):19–56
2. Müller G, Krötz G, Niemann E (1994) SiC for sensors and high-temperature electronics. Sens Actuators A Phys 43(1–3):259–268, May
3. Okojie R, Ned A, Kurtz A (1997) Characteristics of a Hermetic 6H-SiC Pressure Sensor at 600C Tech. Dig. 1997. In: K. Wise, S. Senturia (eds) Int. Conf. Solid State Sensors and Actuators. Chicago IL, June 16–19, p.1407
4. Mehregany M, Zorman C (1999) SiC MEMS: opportunities and challenges for applications in harsh environments. Thin Solid Films 355–356:518–524, 1 November
5. Dong Y, Zorman C, Molian P (2003) Femtosecond pulsed laser micromachining of 3C-SiC structures based on a laser-induced defect-activation process. J Micromech Microeng 13(5):680–685
6. Chichkov B-N, Momma C, Nolte S, Alvensleben F, Tunnermann A (1996) Femtosecond, picosecond, and nanosecond laser ablation of solids. Appl Phys A 63(2):109–115
7. Ozono K, Obara M, Usui A, Sunakawa H (2001) High-speed ablation etching of GaN semiconductor using femtosecond laser. Opt Comm 189:103–106
8. Bonse J, Rudolph P, Kruger J, Baudach S, Kautek W (2000) Femtosecond pulse laser processing of TiN on silicon. Appl Sur Sci 154–155:659–663
9. Liu X, Du D, Mourou G (1997) Laser ablation and micro-machining with ultra-short laser pulses. IEEE J Quant Electron 33 (10):1706–1716
10. Ameer-Beg S, Perrie, W (1998) Femtosecond laser microstructuring of materials. Appl Surf Sci 127–129:875–880
11. Perrie W et al (2005) Femtosecond micro-structuring of alumina ceramic. Appl Surf Sci 258:213–217
12. Perrie W, Gilla M, Robinson B, Foxa P, O'Neil W (2004) Femtosecond laser micro-structuring of aluminum under helium. Appl Surf Sci 230:50–59
13. Robinson GM, Jackson MJ (2006) Femtosecond laser machining of aluminum surfaces under controlled gas atmospheres. J Mater Eng Perform 15(2):155–159
14. Sun J, Longtin JP (2001) Inert gas beam delivery for ultrafast laser micromachining at ambient pressure. Appl Surf Sci 89(12):8219–8223
15. Zoppel S, Farsari M, Merz R, Zehetner J, Stangl G, Reider G, Fotakis C (2006) Laser micro machining of 3C-SiC single crystals. Microelectron Eng 83:1400–1402
16. Toyoda K, Midorikawa K (2001) Micromachining of SiC by femtosecond ablation. Pacific Rim Conference on Lasers and Electro-Optics, CLEO - Technical Digest 2:II286–II287
17. Zorman C (2002) Deposition of 3C-SiC films on 100 mm diameter Si(100) wafers in large-volume LPCVD furnaces. Electrochem Solid-State Lett 5(10):G99
18. Zhang J, Sugioka K, Wada S, Tashiro H, Toyoda K (1997) Direct photoetching of single crystal SiC by VUV-266 nm multiwavelength laser ablation. Appl Phys A 64(4):367–371
19. Pearton S (2002) In: Zetterling C-M (ed) Process technology for silicon carbide devices, London, INSPEC, 2002 p 85
20. Gudde J, Hohlfeld J, Muller J, Matthias E (1998) Damage threshold dependence on electron-photon coupling in Au and Ni films. Appl Sur Sci 127–129:40–45
21. Bulgakova N, Burakov V, Meshcheryakov Y, Stoian R, Rosenfeld A, Hertel I (2007) Theoretical models and qualitative interpretations of fs-laser material processing. J Laser Micro/Nanoengineering 2 (1):76
22. Von der Linde D, Schuler H (1996) Breakdown threshold and plasma formation in femtosecond laser-solid interactions. J Opt Soc Am B 13:216–222
23. Alexander, QW, Ihtesham HC, Xianfan X (2006) Plasma formation in fused silica induced by loosely focused femtosecond laser pulse. Appl Phys Lett 88(11):111502
24. Auguste T et al (1992) Defocusing effects of a picosecond terawatt laser pulse in an under dense plasma. Opt Commun 89:145–148
25. Rae SC (1993) Ionization-induced defocusing of intense laser pulses in high-pressure gases. Opt Commun 97:25–28
26. Gibbon P (2005) Short Pulse Laser Interactions with Matter: An Introduction. Imperial College Press
27. Perez D, Lewis L (2002) Ablation of solids under femtosecond laser pulses. Phys Rev Lett 89(25):25504
28. Shank C, Yen R, Hirlimann C (1983) Femtosecond-time-resolved surface structural dynamics of optically excited silicon. Phys Rev Lett 51(10):900–902
29. Rousse A, Rischel C, Fourmaux S, Uschmann I, Sebban S, Grillon G, Balcou P, Förster E, Geindre J, Audebert P, Gauthier J, Hulin D (2001) Non-thermal melting in semiconductors measured at femtosecond resolution. Nature 410:65–68
30. Stampfli P, Bennemann K (1994) Time dependence of laser-induced femtosecond lattice instability of Si and GaAs fRole of longitudinal optical distortions. Phys Rev B 49 (11):7299–7305
31. Kelly R, Miotello A (1997) On the mechanisms of target modification by ion beams and laser pulses. Nucl Instr Meth B 122:374–400
32. Bulgakova N, Bourakov I (2002) Phase explosion under ultra-short pulsed laser ablation: modeling with analysis of metastable state of melt. Appl Surf Sci 197–198:40–45
33. Sokolowski-Tinten K, Bialkowski J, Cavalleri A, von der Linde D, Oparin A, Meyer-ter-Vehn J, Anisimov S (1998) Transient states of matter during short pulse laser ablation. Phys Rev Lett 81 (1):224–227
34. Lorazo P, Lewis L, Meunier M (2006) Thermodynamic pathways to melting, ablation, and solidification in absorbing solids under pulsed irradiation. Phys Rev B 73:134108
35. Miotello A, Kelly R (1999) Laser-induced phase explosion: new physical problems when a condensed phase approaches the thermodynamically critical temperature. Appl Phys A Suppl 69: S67
36. Stoian R, Ashkenasi D, Rosenfeld A, Campbell E (2000) Coulomb explosion in ultrashort pulsed laser ablation of Al_20_3. Phys Rev B 62(19):13167–13172
37. Henyk M, Costache F, Reif J (2002) Femtosecond laser ablation from sodium chloride and barium flouride. Appl Surf Sci 186:381
38. Tamura H, Kohama T, Kondo K, Yoshida M (2001) Femtosecond-laser-induced spallation in aluminum. J Appl Phys 89(6):3520–3522
39. Nakata Y, Okada T, Maeda M (2003) Nano-size hollow bump array generated by single femtosecond laser pulse. Jpn J Appl Phys 42(12A):L1452–L1454
40. Korte F, Koch J, Chichkov B (2004) Formation of microbumps and nanojets on gold targets by femtosecond pulses. Applied Physics A 79(4–6):879–881

41. Meshcheryakov Y, Bulgakova N (2006) Thermoelastic modeling of microbump and nanojet formation on nanosize gold films under femtosecond laser irradiation. Appl Phys A 82 (2):363–368
42. Eliezer S, Eliaz N, Grossman E, Fischer D, Gouzman I, Henis Z, Pecker S, Horovitz Y, Fraenkel M, Maman S, Lereah Y (2004) Synthesis of nanoparticles with femtosecond pulses. Physical Review B 69:144119
43. Bulgakova N, Bulgakov A (2001) Pulsed laser ablation of solids: transition from normal vaporization to phase explosion. Appl Phys A 73:199–208
44. von der Linde D, Sokolowski-Tinten K (2000) The physical mechanisms of short-pulse laser ablation. Appl Surf Sci 154–155:1–10
45. Song K, Xu X (1998) Explosive phase transformation in excimer laser ablation. Applied Surface Science 127–129:111–116
46. Henyk M, Wolfframm D, Reif J (2000) Ultra short pulse induced charged particle emission from wide bandgap crystals. Appl Surf Sci 168:263–266
47. Cheng H, Gillaspy J (1997) Nanoscale modification of silicon surfaces via Coulomb explosion. Phys Rev B 55:2628
48. Stoian R, Rosenfeld A, Ashkenasi D, Hertel I, Bulgakova N, Campbell E (2002) Surface charging and impulsive ion ejection during ultrashort pulsed laser ablation. Phys Rev Lett 88:97603
49. Roeterdink W, Juurlimk L, Vaughan O, Dura Diez J, Bonn M, Kleyn A (2003) Coulomb explosion in femtosecond laser ablation of Si(111). Appl Phys Lett 82(23):4190–4192
50. Schneider D, Briere M (1996) Investigations of interactions of highest charge state ions with surfaces. Phys Scr 53(2):228–242
51. Itabashi N et al (1995) Desorption of Ga and As atoms from GaAs surface induced by slow multiply charged Ar ions. Jpn J Appl Phys Part 1 34:6861–6865
52. Herrmann R, Gerlach J, Campbell E (1997) Molecular dynamics of laser ablation of silicon. Nucl Instrum Methods Phys Res B 122:401–404
53. Herrmann R, Gerlach J, Campbell E (1998) Ultrashort laser ablation of silicon: an MD simulation study. Applied Physics A 66 (1):35–42
54. Ozkan A, Malshe A, Railkar T, Brown W, Shirk M, Molian P (1999) Femtosecond laser-induced periodic structure writing on diamond crystals and microclusters. Appl Phys Lett 75(23):3716–3718
55. Borowiec A, Haugen H (2003) Sub-wavelength ripple formation on the surfaces of compound semiconductors irradiated with femtosecond pulses. Appl Phys Lett 82(25):4462–4464
56. Yasumaru A, Miyazaki K, Kiuchi J (2003) Femtosecond-laser-indcued nanostructure on hard thin films of TiN and DLC. Appl Phys A 76(6):983–985
57. Pedraza A, Fowlkes J, Guan Y (2003) Surface nanostructuring of silicon. Appl Phys A 77(2):277–284